HHS Public Access

Author manuscript

Exp Neurol. Author manuscript; available in PMC 2021 September 01.

Published in final edited form as:

Exp Neurol. 2020 September ; 331: 113354. doi:10.1016/j.expneurol.2020.113354.

Chronic Defects in Intraspinal Mechanisms of Spike Encoding by Spinal Motoneurons Following Chemotherapy

Stephen N. Housley[1], **Paul Nardelli**[1], **Randal K. Powers**[3], **Mark M. Rich**[4], **Timothy C. Cope**[1,2]

[1]School of Biological Sciences, Georgia Institute of Technology, Atlanta, GA, 30318

[2]Coulter Department of Biomedical Engineering, Georgia Institute of Technology, Atlanta, GA, 30318

[3]Department of Physiology and Biophysics, University of Washington, Seattle, WA

[4]Department of Neuroscience, Cell Biology and Physiology, Wright State University, Dayton, OH, 45435

Abstract

Chemotherapy-induced sensorimotor disabilities, including gait and balance disorders, as well as physical fatigue often persist for months and sometimes years into disease free survival from cancer. While associated with impaired sensory function, chronic sensorimotor disorders might also depend on chemotherapy-induced defects in other neuron types. In this report, we extend consideration to motoneurons, which, if chronically impaired, would necessarily degrade movement behavior. The present study was undertaken to determine whether motoneurons qualify as candidate contributors to chronic sensorimotor disability independently from sensory impairment. We tested this possibility *in vivo* from rats 5 weeks following human-scaled treatment with one of the platinum-based compounds, oxaliplatin, widely used in chemotherapy for a variety of cancers. Action potential firing of spinal motoneurons responding to different fixed levels of electrode-current injection was measured in order to assess the neurons' intrinsic capacity for stimulus encoding. The encoding of stimulus duration and intensity corroborated in untreated control rats was severely degraded in oxaliplatin treated rats, in which motoneurons invariably exhibited erratic firing that was unsustained, unpredictabl e from one stimulus trial to the next, and unresponsive to changes in current strength. Direct measurements of interspike oscillations in membrane voltage combined with computer modeling pointed to aberrations in subthreshold conductances as a plausible contributor to impaired firing behavior. These findings authenticate impaired spike encoding as a candidate contributor to, in the case of motoneurons, deficits in mobility and fatigue. Aberrant firing also becomes a deficit worthy of testing in other CNS neurons as a potential contributor to perceptual and cognitive disorders induced by chemotherapy in patients.

Corresponding author: Timothy C. Cope, School of Biological Sciences and School of Biomedical Engineering, Georgia Institute of Technology, 555 14th St. NW., Atlanta, GA, 30318, tim.cope@gatech.edu.

Keywords

Chemotherapy; central nervous system; CNS; motoneurons; firing behavior; encoding; subthreshold oscillations; impaired excitability; rate-modulation; computer modeling

Introduction

Sensorimotor disabilities induced by chemotherapy often persist months and sometimes years into disease free survival from cancer [1–3]. Disabilities include gait and balance disorders, as well as physical fatigue among other patient complaints related to movement [4–6]. Independent of the potential contributions of neurodegeneration, our preclinical studies of a common-use anticancer platinum-based compound, oxaliplatin (OX) reveal defects in sensory signaling[7–9]. While associated with impaired sensory function, chronic movement disorders might also depend on OX-induced defects in other neuron types. In this report, we extend consideration to motoneurons[10], which, if chronically impaired, would necessarily degrade movement behavior.

Motoneurons demonstrate susceptibility to OX effects, as do primary sensory neurons[11], by firing spontaneously during and for several hours following acute administration of OX[12–15]. For sensory neurons, these early acute affects transition over time from exaggerated to reduced activity, consistent with the decline in sensorimotor function[7–9]. Whether changes in motoneurons follow a similar time course is unknown, or indeed, whether motoneurons express any abnormality that persists chronically within the intact central nervous system of living animals following a full treatment course of chemotherapy. This gap in knowledge impedes mechanistic understanding needed to develop effective rehabilitation, since addressing sensory defects will prove insufficient to restore sensorimotor function if motoneurons are also impaired.

The present study was undertaken to determine whether motoneurons qualify as candidate contributors to chronic sensorimotor disability independently from sensory impairment. Rats were studied five weeks after receiving a human-scaled dose of one of the platinum-based compounds, oxaliplatin (OX), used in 50% of all adjuvant treatment of cancer worldwide. By taking advantage of the experimental access to the spike encoding elements of α-motoneurons within the intact spinal cord of living animals, we provide the first evidence that chemotherapy chronically and severely impairs the intrinsic capacity of motoneurons to regulate firing responses, which were erratic, unpredictable and generally suppressed. Since motoneuron firing plays a deterministic role in translating CNS motor commands into muscle contraction, these firing deficits would necessarily produce movement disorders and fatigue of the sort experienced by cancer survivors during the so-called coasting period when patient symptoms continue or even worsen. Our findings also raise the possibility that disabilities in perception and cognition might result from chemotherapy-induced defects in the central integrative properties of other CNS neuron types.

Methods

Animal Care

All procedures and experiments were approved by the Georgia Institute of Technology Institutional Animal Care and Use Committee or the Wright State University Laboratory Animal Care and Use Committee. Adult female rats (250–350g) were studied in terminal experiments only and were not subject to any other experimental procedures. All animals were housed in clean cages and provided food and water ad libitum in a temperature- and light-controlled environment.

Chemotherapy treatment

Oxaliplatin (OX) was injected i.p. once a week (10mg/Kg, 1 ml 5% dextrose in DMSO) to achieve a cumulative dose of 70 mg/Kg over 7 weeks (Fig. 1a), which scales to a human dose of 420mg/m^2 (conversion based on rat body surface area and K_m= 6)[16,17]. This dose minimizes nerve degeneration in patients[18,19]. Throughout treatment, rats were frequently monitored for pain or distress [8]. No individual rat reached set criteria established for early removal from the study.

In Vivo Surgical Procedures and Intracellular Recordings

Terminal *in vivo* experiments were performed 5 weeks after achieving clinically relevant chemotherapy doses[8,9]. Experiments were designed to measure the electrical properties and firing characteristics of individual motoneurons *in vivo*. Surgical and recording techniques used in these studies have been described in previously published reports from this laboratory[7,20–23].

Briefly, data were collected from medial gastrocnemius motoneurons (MG) in rats anesthetized by inhalation of isoflurane (1.2–1.5% mixed in 100% O2) and fixed in a rigid recording frame. Properties of MG were measured by intracellular recording with glass microelectrodes (K-acetate, 5–10 MΩ). Microelectrodes were advanced through the dorsal spinal cord until antidromic APs, generated by electrical stimulation of the medial gastrocnemius nerve (0.04-ms pulses, 1 Hz), were identified in the microelectrode voltage records. All recordings were performed using an Axoprobe 1A (Sunnyvale, CA) amplifier in either bridge or DCC mode. APs were initiated in MG motoneurons by injecting suprathreshold depolarizing current (square pulses lasting ≥100 ms) directly into motoneuron soma within the spinal cord. Intracellular measures were recorded or derived to characterized the intrinsic excitability of MG motoneuron: a series of antidromic action potentials (APs), a series of 50-ms current pulses of different amplitude to determine rheobase, a series of 1-ms, suprathreshold current pulses were applied to elicit direct APs and afterhyperpolarizations (AHPs), followed by a series of ±5 nA, 500-ms current steps to measure input resistance. Motoneuron firing rates in response to microelectrode current injection were used to measure the gain of the motoneuron frequency-current relation (f-I slope)[24]. Repetitive firing during 5-s pulses was assessed at several different levels of current. These parameters reflect the translation of current into firing rates by motoneurons and are standard indices of the intrinsic excitability of motoneurons. Respiratory and cardiac movement artifact of the rats sometimes made it difficult to maintain stable somatic

penetrations. Therefore, a paralytic agent (pancuronium bromide) was occasionally administered intraperitoneally, and paralysis was maintained throughout the experiment.

Bayesian data analysis

Statistical techniques used in these studies have been described in a previously published report from this laboratory[25]. Briefly, analyses focused on motoneuron spiking probability, firing characteristics, and rate-modulation for both OX and control groups. Because of inconsistent spiking behavior in OX motoneurons, all analyses utilized 20ms temporal bins in order to effectively characterize extended periods without spiking activity. Traditional analyses focused on interspike intervals underestimate information loss by counting these periods as one event whereas control motoneurons frequently had many tens or hundreds of events. Applying this approach to control motoneuron populations reproduces the expected behavior seen previously in multiple reports, giving confidence in its validity[26–29]. We employed Bayesian models to compute parameters in order to explicitly test our working hypothesis that OX chronically impairs motor unit function. We empirically derived the full joint posterior probability distributions of model parameters simultaneously and directly examined the posterior distributions[30–32], imparting noteworthy advantages over frequentist analysis[31–33]. Bayesian inference was performed by inspecting the highest density interval (HDI), such that values inside the 95% of the HDI are more credible than outside values[33].

HDI was used to make unbiased decisions on parameter values. All models were developed in fully Bayesian framework with the *rstanarm* package (2.18.1)[34] in the R environment (3.5.0)[35]. For intercepts and predictors, we use Student's *t*-distribution with mean zero and four degrees of freedom as the prior distribution. The scale of the prior distribution is 10 for the intercept and 2.5 for the predictors. Each model was run with four independent chains for 1,000 warm-up and 4,000 sampling steps. For all parameters, the number of effective samples was >500. Convergence was assessed and assumed to have reached the stationary distribution by ensuring that the Gelman–Rubin shrinkage statistic for all reported parameters was <1.05[36]. We report the expected mean parameter values alongside 95% credible intervals using (HDI).

In Silico Motoneuron Experiments

We used a single compartment model of a rat motor neuron implemented in NEURON 7.6 to simulate the behavior of motoneurons from control animals and those treated with OX. The model was similar to those described in Golomb et al. (2007)[37] and Sciamanna and Wilson (2011)[38], in that the critical components controlling the pattern of discharge were a slowly-inactivating, low threshold Kv1 current, a fast Na current that included a variable persistent component and a small amount of noise[39]. The model also contained a delayed rectifier K current responsible for AP repolarization, a calcium-activated K current responsible for the afterhyperpolarization, a hyperpolarization-activated mixed cation current and a leak conductance. Details of the model will be made available on the MODELDB website (https://senselab.med.yale.edu/ModelDB/). In our model, the Hodgkin-Huxley-type Na model used by Golomb et al. (2007)[37] and Sciamanna and Wilson(2011) [38] was replaced by a ten-state kinetic gating model adapted from the eight-state model described by Schmidt-Hieber and Bischofberger (2010)[40] by adding two slow inactivated states; one entered from

the open state and one from a fast-inactivated state. Variations in the amount of persistent Na current (i.e., the proportion of channels in the open state under steady-state conditions) were produced either by changing the rate at which channels entered the fast-inactivated states by changing the voltage dependence of fast-inactivation (green arrows in Fig 1A) or by changing the rate of entry into slow-inactivated states (red arrows in Fig 1A). Figure 1B – D shows the effects of a 5 mV (blue) or 10 mV (green) hyperpolarizing shift in fast inactivation or a doubling of the rate of entry into slow inactivated states (red) on the steady-state voltage dependence of the proportion of channels in the open state (B), fast-inactivated states (C) and slow inactivated states (D). In addition, we then systematically varied the maximal Kv1 conductance along with the level of injected current to reveal regions in parameter space associated with irregular firing (coefficients of variation of interspike intervals (ISI)> 0.2; values for motor neurons are typically <0.229. For a given combination of conductance values we sampled a wide distribution of current levels (1nA apart) to best validate model performance on the distribution of experimental recordings.

3. Results

3.1 Characterizing Erratic Firing

3.1.1. Chemotherapy Disrupts Repetitive Firing of Motoneurons—Effects of chemotherapy on repetitive firing and other biophysical properties of motoneurons recorded *in vivo* were tested by comparing data taken from control rats receiving no prior treatment (n=5) and from OX rats (n = 6) studied 5 weeks after receiving a clinically relevant cumulative dose of oxaliplatin (70mg/kg) (Methods). Figure 2A shows representative data for one motoneuron from each group in response to 5 sec pulses of constant current injection applied by current clamp. Control motoneurons (7/7) responded with repetitive firing that was regular and consistently sustained throughout current injection as described in earlier studies of motoneurons in control rats[21,22,26,29,41,42]. By contrast, all motoneurons (8/8) sampled from OX rats, hereafter designated OX motoneurons, responded with erratic firing, defined by APs occurring sporadically or in irregular bursts interrupted by varying durations of no firing as represented by records from one OX motoneuron in Fig. 2A. The disorder found for firing patterns within single 5 sec stimulus trials extended across replicate trials, which exhibited different patterns of firing irregularity from one trial to the next.

The effect of chemotherapy was evident in pooled group comparisons of firing parameters measured at matched current intensities (6–8 nA > rheobase current). In one comparison, a hierarchical Bayesian binomial model was applied to empirically derive the probability (posterior probability distribution) of an action potential occurrence compiled over 10 ms bins spanning the duration of the 5 sec current pulses at matched current-injection trials for control and OX motoneurons (see Methods). This analysis demonstrated a 5.875 fold reduction (95%HDI: 5.7–6.05) in probability of AP occurrence in OX compared to control motoneurons. Reduced firing probability resulted in a significant reduction in the number of APs (Fig. 2B), which translated to a significant reduction in mean firing rates (Fig. 2C). To characterize temporal irregularity in firing, we calculated the coefficient of variation in firing rate, which revealed a 7-fold increase for OX as compared to control motoneurons (Fig. 2D). In summary, OX motoneurons responded to stationary pulses of current injection with

irregular firing that was unpredictable over both short- and long-time scales in striking contrast to the steady and sustained firing responses of control motoneurons.

3.1.2. Chemotherapy Eliminates Firing Rate Modulation in Motoneurons—

Motoneurons were examined for their intrinsic capacity to modulate firing rate in response to varying current intensities. A representative case for control motoneurons in Fig. 3 illustrates that firing rate increased together with current strength as expected[26,29,41,43]. Note that inconsistent firing induced at the beginning of the trial (top trace) at the lowest current strength (4 nA above rheobase current), was completely resolved at higher strengths. By contrast, the firing exemplified for OX motoneurons in Fig. 3 shows little evidence of firing rate modulation and a failure to achieve regular firing at all current strengths studied (up to 14 nA above rheobase current).

Typical of CNS neurons, motoneurons normally modulate firing frequency by integrating synaptic current, or in response to artificial current injection employed in the present study[29]. The frequency-current (F-I) relationship received special attention here, because of its critical role in controlling muscle force and movement[44]. All control motoneurons increased firing rate consistently across multiple trials of increasing current intensity (Fig. 3, 4A). The F-I relationship for the pooled sample of motoneurons was 3.46 (95%HDI: 3.44–3.48) pulses per second (pps) per nA, similar to that reported in similar studies of rat motoneurons[29]. By contrast, OX motoneurons exhibited virtually no modulation of firing rate in response to increasing current (Fig. 3, 4C).

Sparse evidence of a positive F-I relation appeared in a few trials (Fig. 4D, motoneurons 2 and 7), but the high density of low firing rates across different current intensities for all OX motoneurons (Fig. 4C, D) indicates the absence of rate modulation in most trials. Overall, the F-I relationship for pooled OX motoneurons was −0.09 (95%HDI: −0.11– −0.07) pps per nA, indicating that OX blunted the capacity for motoneurons to modulate firing rate over 5 sec current trials. These results demonstrate that OX severely impairs a key regulator of motoneuron input-output behavior.

3.2 Biophysical Measures in Relation to Erratic Firing

3.2.1. Chemotherapy Does Not Alter Characteristics of Single Antidromic APs.—

Passive properties of motoneurons (resting potential and input resistance) and the characteristics of single antidromic APs were examined in attempt to advance mechanistic insight into impaired firing. All properties listed in Table 1 for control motoneurons were similar to those previously reported[21,22,26,27,29,41–43,45], and none were significantly different for OX motoneurons. Specifically, neither resting membrane potential nor input conductance showed differences suggestive of a treatment effect on K leak conductance or reversal potential. Similarities in properties of antidromic APs suggested normalcy of underlying mechanisms. Group comparison of maximum dV/dt for AP upstroke or downstroke suggested no effect of OX on, respectively, Na or K channel density, voltage dependence, and/or inactivation[45]. By these measures of passive and active membrane properties, neuronal excitability exhibited no chronic effect OX treatment. This conclusion is further supported by group similarity of a holistic measure of excitability, namely AP current

threshold, i.e. rheobase current. Preservation of relative recruitability has important functional consequences as one of two primary determinants in controlling muscle force and movement, with rate modulation being the other.

3.2.2. Sodium Channel Inactivation Does Not Predict Erratic Firing—The apparently normal expression of Na channel inactivation observed for single action potentials, does not rule out impairment in the dynamic behavior it exhibits during repetitive firing as a possible contributor to abnormal firing in OX motoneurons. In support of this possibility, Na channel inactivation has been linked to deficits in sustained firing in pathological conditions, and is therefore a plausible candidate for erratic firing observed with OX treatment. We reasoned that if Na channel inactivation contributes to defective repetitive firing, then the degree of inactivation should be greatest prior to pauses in firing, and relief of inactivation should occur prior to resumption of firing. We estimated the degree of sodium channel inactivation by measuring the maximal rate of rise of action potentials ($dV/dt^{46,47}$) during repetitive firing in response to a 5s suprathreshold current step(Fig 5A–B)[42]. Analyses of OX motoneurons focused on APs just preceding pauses in firing and those immediately following and several seconds after the resumption of firing (Fig 5B, grey and dotted traces and arrows) in OX motoneurons (cf Figs. 5B and 5D) and action potentials taken at regular intervals in control (Fig 5A–C). In comparison with APs preceding a pause, ones occurring when repetitive firing resumed had significantly smaller values for dV/dt (Fig. $5D_1$ 210 ± 14 vs. 243 ± 14 mV/ms; 95% HDI do not cross) and amplitude (48.9 ± 2.9 vs. 55.1 ± 2.5 mV; 95% HDI do not cross) as compared to control (Fig. $5C_1$). In other words, AP dV/dt, and inferred Na inactivation did not predict either the stop or restart of repetitive firing in OX motoneurons. Consistent with the independence of erratic firing behavior from dV/dt, Fig. 5F shows dissimilar firing patterns across increase levels of current injection occurring together with relatively little change in dV/dt, possibly because moderate firing rates were not sustained. By contrast, control motoneurons were able to sustain firing at high rates despite relatively lower AP dv/dt at higher levels of current injection (Fig. 5E).

3.2.3. Abnormalities in Subthreshold Behavior During Repetitive Firing—Given the lack of changes in either motoneuron electrical properties or characteristics of single antidromic APs, we considered the possibility that subthreshold currents responsible for the approach to AP threshold in repetitive firing might be the underlying biophysical mechanism perturbed by OX. Examination of the interspike membrane voltages revealed high-frequency (>100Hz) oscillations associated with erratic firing (Fig. 6A) as opposed to the smooth, predictable approaches observed in control motoneurons during regular firing (Fig. 6A). Membrane oscillations were observed both independently of and immediately preceding the resumption of repetitive firing. Analyses of the approach to AP threshold revealed that resumption of firing was consistently preceded by pre-spike hyperpolarizing events (Fig. 6A arrows). Membrane voltages approaching spike threshold were spike-triggered average over all APs in a 5 second trial for all control and OX motoneurons. In contrast with control motoneurons, the rate of depolarization was significantly slower and interrupted by a discreet, transient hyperpolarization just before action potential onset, i.e. a pre-spike hyperpolarization (Fig. 6B–C: 95%HDI do not cross).

Oscillations in membrane potential during firing have been suggested to be due to the competing influence of inward and outward currents mediated by fast, voltage-dependent currents that are activated in the subthreshold range[37]. Subthreshold currents determine whether the motoneuron will reach AP threshold, such that oscillations may indicate dysregulation of the currents responsible for repetitive firing. Both Na^+ and CaV1.3-type calcium channels contribute to a low-threshold persistent inward current (PIC) in motoneurons; however, the kinetics of the CaPIC appear too slow to be responsible for the fast oscillations identified in OX motoneurons. This left the persistent inward component of the Na current (NaPIC) and low threshold Kv1-type potassium currents as the most likely candidates[28,48]. We hypothesized that erratic firing emerges from a reduction in the ratio of inward to outward currents (NaPIC/Kv1 ratio) and associated oscillations that introduce inconsistency in reaching AP threshold. Imbalances in subthreshold currents are held responsible for membrane oscillations in a number of different neurons, including motoneurons[21,49].

3.3 Modeling Intrinsic Encoding Mechanisms Underlying Erratic Firing

3.3.1. Modulation of Subthreshold Kinetics Reproduces Erratic Firing.—

To test this hypothesis, we constructed a model of spike encoding by rat motoneurons in silico to determine whether altering the NaPIC/Kv1 ratio was sufficient to reproduce unpredictable firing present in OX motoneurons. Figure 7 shows that the qualitative behavior of the model matched certain features of the experimental data, i.e., low firing rate variability for the control simulation and irregular stuttering firing over a range of injected current levels for the OX simulation. Figure 8 provides a more quantitative assessment of the relation between injected current level and mean firing rate and interspike interval variability (coefficient of variation, CoV) for the experimental (A and B) and simulated (C - F) data. The control simulation (Fig. 8C) reproduced experimental firing behaviors over a large range of injected current levels, i.e., a transient increase in CoV just above rheobase and subsequent reduction thereafter and monotonic increase in firing rate. We then modelled OX motoneurons by systematically altering the NaPIC/Kv1 ratio which reproduced erratic firing that was not completely rescued by increasing excitatory drive (Fig. 8B). Comparison of model derived ISI CoV to those observed experimentally revealed both increase rapidly above rheobase and remain elevated, although experimental data were approximately two- to three-fold larger. Nonetheless, modelled firing rates increased monotonically with the level of injected current, in contrast to the experimental data (see Fig. 4B and 8B). By tuning both Kv1 and NaPIC conductances, we determined that altered firing rates observed in OX motoneurons were reproduced over a range of lower (0.006 S/cm2: Figure 9E) and higher (0.008 S/cm2: Fig. 8F) Kv1 conductances. At low Kv1 conductances, a hyperpolarizing shift in the inactivation curve of NaPIC by either 5 (blue) or 10 mV (green) lead to the CoV recovery at higher injected currents (Fig. 8E), whereas these alterations had little effect at high Kv1 conductances (Fig. 8F). However, at these higher simulated levels of Kv1 model motoneurons failed to generate more than one spike until injected current levels were 5 – 12 nA above the rheobase value (9–10 nA in the OX simulations), in contrast to the experimental OX data.

3.3.2. Modeling Effects of Subthreshold Kinetics on Spike Encoding—We then tested whether altering the NaPIC/Kv1 ratio was sufficient to reproduce erratic subthreshold kinetics present in OX motoneurons. Voltage records from simulated motoneuron reproduced the two main features observed experimentally: subthreshold oscillations in membrane potential and amplified pre-spike hyperpolarization (Fig. 9A). We then analyzed the average membrane voltages approaching spike threshold (spike -riggered average) over all spikes in a 5 second trial from simulated control and OX motoneurons. We found a remarkable degree of concordance with averages obtained from the experimental data (Fig. 6). Collectively, the results of computer simulations indicate that a reduction in the NaPIC/Kv1 ratio is sufficient to reproduce many of the features of the defects in motoneuron repetitive firing present following OX treatment and suggest this as one candidate biophysical mechanism that may be directly or indirectly targeted by OX.

Discussion

Here we present the first evidence that chemotherapy chronically impairs firing behavior in a class of neurons within the intact central nervous system of a living mammal. For spinal motoneurons, we found that repetitive firing was unsustainable and unpredictable in rats five weeks following a human-scaled treatment course of OX. The firing defects originated in the motoneurons' central integrative components responsible for spike encoding, and direct measurement coupled with computer simulations identified an imbalance of subthreshold currents as a candidate mechanism. For motoneurons, erratic firing would unavoidably generate movement disorders, e.g. clumsiness and fatigue, experienced by patients following chemotherapy with OX and other anticancer compounds[2,3]. If expressed more generally across other types of CNS neurons, defects in the central integrative properties that encode action potential firing becomes a likely source of a broader set of patient symptoms induced by chemotherapy, including disorders in movement as well as in perception and cognition.

Biophysical mechanism(s) underlying erratic firing

Repetitive firing in neurons can be elicited either by steady depolarizing synaptic input or by injected current. The relation between excitatory input and firing is governed not only by the currents underlying the action potentials and afterpotentials but also by those that are active at membrane potentials more negative than action potential threshold (subthreshold currents). These subthreshold currents consist of both non-voltage gated (leak) currents and voltage-gated currents. It has been suggested that both subthreshold depolarizing and subthreshold hyperpolarizing current interact to cause the oscillations in membrane potential that can accompany irregular or bursting discharge in neurons in response to current injection[37,38,50,51]. High-frequency oscillations of the type seen in the present experiments and previous descriptions of septic motoneurons[21,22,52] and mouse motoneurons[51] require subthreshold currents with rapid kinetics (time constants < 5 ms). The most likely depolarizing and hyperpolarizing conductances contributing to oscillations and irregular firing are the NaPIC and Kv1 potassium channels. Both NaPIC and Kv1 are first activated below threshold and have rapid kinetics. Low NaPIC/Kv1 ratios are expected to lead to irregular firing whereas high ratios are thought to underlie more regular discharge. Both simulation[37] and experimental results[53] suggest that reductions in NaPIC can disrupt steady

repetitive firing. Conversely, block of Kv1 currents can convert irregular to regular discharge[38,50].

We hypothesized that the defect in repetitive firing in motor neurons from OX rats was due to reduction in the NaPIC/Kv1 ratio. This possibility was explored using computer simulation. When the NaPIC/Kv1 ratio is high, simulation produced rapid depolarization toward action potential threshold and a high F-I gain (a high firing rate for a given current injection) and stable firing without pauses. When the ratio was low there was inconsistent repetitive firing at lower rates and the f-I gain was reduced. However, we were not able to reproduce the near complete loss of the f-I relationship in OX neurons. Similarly, other simulation work suggests that alterations in NaPIC/Kv1 ratio alone are only able to disrupt regular firing over a narrow range of current strengths[37,51]. This suggests that additional abnormalities, yet to be determined, contribute to the disruption of repetitive firing.

In this study we did not directly test the mechanisms suggested by modelling for their relevance to defects in repetitive firing measured *in vivo*. However, in previous studies of sepsis, we found similar defects in repetitive firing to those reported here, consisting of subthreshold oscillations in membrane potentials, pauses in repetitive firing and reduced F-I gain[21,22,42]. In septic motoneurons we applied dynamic clamp to increase the ratio of depolarizing to hyperpolarizing subthreshold current and this was sufficient to normalize repetitive firing[21]. Conversely, reducing the ratio, could cause the septic pattern of firing in motor neurons from healthy rats[21]. These data demonstrated that reduction in the ratio of depolarizing to hyperpolarizing subthreshold currents was sufficient to explain the defect in firing of motoneurons.

Origins of Chronic Defects in Motoneuron Firing

The incipient event(s) in chemotherapy induction of motoneuron firing defects is(are) yet to be determined, but several possibilities bear consideration. Direct chemotoxic damage of spike encoding mechanisms within the central nervous system stands as a plausible initiator of motoneuron firing defects. There is ample experimental evidence that contact with anticancer agents, including platinum-based compounds have acute neurotoxic effects that change the excitability of neurons[54]. Direct exposure to OX is known to impair neuron ion channels, including NaV1.6[55] and Kv1[56,57], which are present in motoneurons[58] and identified in our simulations for their potential to produce the observed firing defects. Neurons extracted from the CNS and studied *in vitro* exhibit a variety of biophysical changes underlying increased excitability and firing when anticancer compounds are infused in the medium[59,60]. Within the CNS, the integrative components, i.e. dendrites, soma, and axon initial segment of motoneurons may encounter platinum-based compounds, which cross the blood brain barrier despite limited permeability to reach low, but finite concentrations in CNS[61–64], and in cerebral spinal fluid of patients after a single systemic administration[62,63,65]. Preclinical study shows that comparably low doses of OX introduced into the CNS have significant effects on neuronal excitability[59,60]. Through direct chemotoxicity, spike encoding defects might reasonably emerge then as platinum concentrations accumulate and persist, because OX may be retained for many years[66].

If not by direct chemotoxicity, then defective spike encoding might be triggered by diverse indirect mechanisms. The possibility of indirect effects gains attention under chronic conditions in patients and in the present studies, wherein complex sequalae and adaptations have time to develop. Motoneurons and other CNS neurons, including trigeminal, geniculate, and preganglionic sympathetic neurons are vulnerable to chemotoxic exposure by extending axons into the periphery where OX concentrations are highest. Through this route, OX might impair a neuron's central spike encoding mechanisms secondarily in response either to axonal transport of OX into the CNS or to the metabolic and structural damage to peripheral axons that is caused by OX[67,68], as it is by disease, e.g. ALS or other neurotoxic compounds used in chemotherapy, e.g. [69–71]. Present findings may appear to challenge the latter possibility, because, consistent with studies of human subjects[72], motor axons sampled here exhibited no detectable abnormality in excitability or action potential long after OX treatment is discontinued. However, OX effects on motor axons are plainly demonstrated by spontaneous firing of motor units recorded within hours after its administration[12–15]. This early hyperactivity might reflect chemotoxic interaction with axonal ion channels[73], or it may be related to upregulation of early immediate genes as observed acutely for cultured motoneurons bathed in the chemotherapeutic compound camptothecin[74]. Regardless of mechanism, transient acute hyperactivity may have the capacity to set into motion mechanisms, including homeostatic compensation mechanisms, which, if dysregulated as proposed for motoneurons in ALS[75–77], could over-compensate to produce the hypo-excitability observed here. Finally, global systemic effects of OX comprise a broad category of candidates capable of inducing impaired spike encoding for neurons in general. Systemic signaling pathways, e.g. oxidative and inflammatory are damaged or activated in ways demonstrated to alter neuronal excitability (e.g. [54,78–87]). Chemotherapy is also shown to influence global regulatory mechanisms capable of altering neural activity through epigenetic control, e.g. increase H3 acetylation and decreased histone deacetylase activity[88,89]. Thus, impaired firing behavior of motoneurons might be collateral damage caused by a variety of cellular mechanisms, e.g. gene expression and post-translational modifications, and regulatory networks, e.g. inflammatory and metabolic pathways, known to have influence over neuronal excitability and behavior. Distinguishing these candidate origins of defective motoneuron firing has potential to identify targets for preventing its occurrence.

Functional Consequences

Erratic firing induced by chemotherapy in any class of CNS neuron has the potential to cause serious consequences for behaviors generated by the neural networks in which they are embedded. This is especially true for motoneurons, which are the final common pathway for the neural commands evoking muscle force to produce movement. Motoneurons normally execute their role by converting synaptic current into regular firing patterns which set the magnitude, stability, and duration of muscle contraction. As a result of chemotherapy-induced impairment to the intrinsic properties of repetitive firing, motoneurons cannot execute this role. Moreover, it's improbable that any adjustment in presynaptic input could compensate, because motoneuron firing pattern and duration varied unpredictably form one stimulus trial to the next. Motoneuron firing that cannot be predicted, sustained, or compensated would severely impair control of movement and might,

therefore, contribute to the chronic disorders of posture, mobility and fatigue experienced by patients treated with chemotherapy. Although no other class of CNS neuron has yet been examined, our study identifies defective neuronal firing as a candidate mechanism underlying impairment of associated neural networks and behaviors. For example, our findings suggest defective firing of neurons in pre-frontal cortex as a possible mechanism underlying the cognitive deficits comprising “chemo-brain” and associated alteration is regional brain activity.

Acknowledgements:

This work was supported by National Cancer Institute (NCI) Grant R01 CA221363.

References

1. Park SB et al. Long-term neuropathy after oxaliplatin treatment: challenging the dictum of reversibility. Oncologist 16, 708–716 (2011). [PubMed: 21478275]
2. Bennett BK et al. Impact of oxaliplatin-induced neuropathy: a patient perspective. Supportive Care in Cancer 20, 2959–2967 (2012). [PubMed: 22426503]
3. Tofthagen C, Donovan KA, Morgan MA, Shibata D. & Yeh Y. Oxaliplatin-induced peripheral neuropathy’s effects on health-related quality of life of colorectal cancer survivors. Supportive Care in Cancer 21, 3307–3313 (2013). [PubMed: 23903798]
4. Vardy J. et al. Fatigue in people with localized colorectal cancer who do and do not receive chemotherapy: a longitudinal prospective study. Annals of Oncology 27, 1761–1767 (2016). [PubMed: 27443634]
5. Marshall TF, Zipp GP, Battaglia F, Moss R. & Bryan S. Chemotherapy-induced-peripheral neuropathy, gait and fall risk in older adults following cancer treatment. Journal of Cancer Research and Practice (2017).
6. Kneis S. et al. Balance impairments and neuromuscular changes in breast cancer patients with chemotherapy-induced peripheral neuropathy. Clinical neurophysiology 127, 1481–1490 (2016). [PubMed: 26350407]
7. Bullinger KL, Nardelli P, Pinter MJ, Alvarez FJ & Cope TC Permanent central synaptic disconnection of proprioceptors after nerve injury and regeneration. II. Loss of functional connectivity with motoneurons. Journal of neurophysiology 106, 2471–2485 (2011). [PubMed: 21832030]
8. Housley SN et al. Cancer Exacerbates Chemotherapy Induced Sensory Neuropathy. bioRxiv, 667105 (2019).
9. Vincent JA et al. A novel path to chronic proprioceptive disability with oxaliplatin: distortion of sensory encoding. Neurobiology of disease 95, 54–65 (2016). [PubMed: 27397106]
10. Binder MD, Heckman C. & Powers RK The physiological control of motoneuron activity. Comprehensive physiology, 3–53 (2010).
11. Li Y. et al. DRG Voltage-Gated Sodium Channel 1.7 Is Upregulated in Paclitaxel-Induced Neuropathy in Rats and in Humans with Neuropathic Pain. Journal of Neuroscience 38, 1124–1136 (2018). [PubMed: 29255002]
12. Webster RG, Brain KL, Wilson RH, Grem JL & Vincent A. Oxaliplatin induces hyperexcitability at motor and autonomic neuromuscular junctions through effects on voltage-gated sodium channels. Br J Pharmacol 146, 1027–1039, doi:10.1038/sj.bjp.0706407 (2005). [PubMed: 16231011]
13. Hill A. et al. Detecting acute neurotoxicity during platinum chemotherapy by neurophysiological assessment of motor nerve hyperexcitability. BMC cancer 10, 451 (2010). [PubMed: 20731872]
14. Lehky T, Leonard G, Wilson R, Grem J. & Floeter M. Oxaliplatin-induced neurotoxicity: acute hyperexcitability and chronic neuropathy. Muscle & nerve 29, 387–392 (2004). [PubMed: 14981738]

15. Wilson RH et al. Acute oxaliplatin-induced peripheral nerve hyperexcitability. Journal of Clinical Oncology 20, 1767–1774 (2002). [PubMed: 11919233]
16. Reagan-Shaw S, Nihal M. & Ahmad N. Dose translation from animal to human studies revisited. The FASEB journal 22, 659–661 (2008). [PubMed: 17942826]
17. Nair AB & Jacob S. A simple practice guide for dose conversion between animals and human. Journal of basic and clinical pharmacy 7, 27 (2016). [PubMed: 27057123]
18. Park SB et al. Chemotherapy-induced peripheral neurotoxicity: A critical analysis. CA: a cancer journal for clinicians 63, 419–437 (2013). [PubMed: 24590861]
19. Grisold W, Cavaletti G. & Windebank AJ Peripheral neuropathies from chemotherapeutics and targeted agents: diagnosis, treatment, and prevention. Neuro-oncology 14, iv45-iv54 (2012).
20. Haftel VK, Bichler EK, Nichols TR, Pinter MJ & Cope TC Movement reduces the dynamic response of muscle spindle afferents and motoneuron synaptic potentials in rat. Journal of neurophysiology 91, 2164–2171 (2004). [PubMed: 14695354]
21. Nardelli P, Powers R, Cope TC & Rich MM Increasing motor neuron excitability to treat weakness in sepsis. Annals of neurology 82, 961–971 (2017). [PubMed: 29171917]
22. Nardelli P, Vincent JA, Powers R, Cope TC & Rich MM Reduced motor neuron excitability is an important contributor to weakness in a rat model of sepsis. Experimental neurology 282, 1–8 (2016). [PubMed: 27118372]
23. Vincent JA et al. Muscle proprioceptors in adult rat: mechanosensory signaling and synapse distribution in spinal cord. Journal of neurophysiology 118, 2687–2701 (2017). [PubMed: 28814636]
24. Powers RK & Binder MD Input-output functions of mammalian motoneurons. Reviews of physiology, biochemistry and pharmacology, 137–263 (2001).
25. Horstman GM, Housley SN & Cope TC Dysregulation of mechanosensory circuits coordinating the actions of antagonist motor pools following peripheral nerve injury and muscle reinnervation. Experimental neurology (2019).
26. Bakels R. & Kernell D. Matching between motoneurone and muscle unit properties in rat medial gastrocnemius. The Journal of physiology 463, 307–324 (1993). [PubMed: 8246185]
27. Beaumont E. & Gardiner P. Effects of daily spontaneous running on the electrophysiological properties of hindlimb motoneurones in rats. The Journal of physiology 540, 129–138 (2002). [PubMed: 11927675]
28. Chatelier A, Zhao J, Bois P. & Chahine M. Biophysical characterisation of the persistent sodium current of the Na v 1.6 neuronal sodium channel: a single-channel analysis. Pflügers Archiv-European Journal of Physiology 460, 77–86 (2010). [PubMed: 20204400]
29. Turkin VV, O'Neill D, Jung R, Iarkov A. & Hamm TM Characteristics and organization of discharge properties in rat hindlimb motoneurons. J Neurophysiol 104, 1549–1565, doi:10.1152/jn.00379.2010 (2010). [PubMed: 20592119]
30. Wagenmakers E-J A practical solution to the pervasive problems ofp values. Psychonomic bulletin & review 14, 779–804 (2007). [PubMed: 18087943]
31. Kruschke J. Doing Bayesian data analysis: A tutorial with R, JAGS, and Stan. (Academic Press, 2014).
32. Kruschke JK Bayesian estimation supersedes the t test. Journal of Experimental Psychology: General 142, 573 (2013). [PubMed: 22774788]
33. Kruschke JK What to believe: Bayesian methods for data analysis. Trends in cognitive sciences 14, 293–300 (2010). [PubMed: 20542462]
34. Gabry J. & Goodrich B. rstanarm: Bayesian applied regression modeling via Stan. R package version 2.18.1 (2018).
35. Team, R. C. (ISBN 3-900051-07-0: URL http://www.R-project.org, 2018).
36. Gelman A. & Rubin DB Inference from iterative simulation using multiple sequences. Statistical science 7, 457–472 (1992).
37. Golomb D. et al. Mechanisms of firing patterns in fast-spiking cortical interneurons. PLoS Comput Biol 3, e156 (2007). [PubMed: 17696606]

38. Sciamanna G. & Wilson CJ The ionic mechanism of gamma resonance in rat striatal fast-spiking neurons. Journal of neurophysiology 106, 2936–2949 (2011). [PubMed: 21880937]
39. Destexhe A, Rudolph M, Fellous J-M & Sejnowski TJ Fluctuating synaptic conductances recreate in vivo-like activity in neocortical neurons. Neuroscience 107, 13–24 (2001). [PubMed: 11744242]
40. Schmidt-Hieber C. & Bischofberger J. Fast sodium channel gating supports localized and efficient axonal action potential initiation. Journal of Neuroscience 30, 10233–10242 (2010). [PubMed: 20668206]
41. Button DC, Gardiner K, Marqueste T. & Gardiner PF Frequency–current relationships of rat hindlimb α-motoneurones. The Journal of physiology 573, 663–677 (2006). [PubMed: 16613880]
42. Nardelli P, Khan J, Powers R, Cope TC & Rich MM Reduced motoneuron excitability in a rat model of sepsis. Journal of neurophysiology 109, 1775–1781 (2013). [PubMed: 23303860]
43. Hamm TM, Turkin VV, Bandekar NK, O'Neill D. & Jung R. Persistent currents and discharge patterns in rat hindlimb motoneurons. J Neurophysiol 104, 1566–1577, doi:10.1152/jn.00380.2010 (2010). [PubMed: 20592117]
44. Enoka RM & Fuglevand AJ Motor unit physiology: some unresolved issues. Muscle & Nerve: Official Journal of the American Association of Electrodiagnostic Medicine 24, 4–17 (2001).
45. Bean BP The action potential in mammalian central neurons. Nature Reviews Neuroscience 8, 451 (2007). [PubMed: 17514198]
46. Brownstone RM, Krawitz S. & Jordan LM Reversal of the late phase of spike frequency adaptation in cat spinal motoneurons during fictive locomotion. Journal of neurophysiology 105, 1045–1050 (2010). [PubMed: 21177992]
47. Miles G, Dai Y. & Brownstone R. Mechanisms underlying the early phase of spike frequency adaptation in mouse spinal motoneurones. The Journal of physiology 566, 519–532 (2005). [PubMed: 15878947]
48. Caldwell JH, Schaller KL, Lasher RS, Peles E. & Levinson SR Sodium channel Nav1. 6 is localized at nodes of Ranvier, dendrites, and synapses. Proceedings of the National Academy of Sciences 97, 5616–5620 (2000).
49. Manuel M. et al. Fast kinetics, high-frequency oscillations, and subprimary firing range in adult mouse spinal motoneurons. J Neurosci 29, 11246–11256, doi:29/36/11246 [pii] 10.1523/JNEUROSCI.3260-09.2009 (2009). [PubMed: 19741131]
50. Hsiao C-F, Kaur G, Vong A, Bawa H. & Chandler SH Participation of Kv1 channels in control of membrane excitability and burst generation in mesencephalic V neurons. Journal of neurophysiology 101, 1407–1418 (2009). [PubMed: 19144742]
51. Iglesias C. et al. Mixed mode oscillations in mouse spinal motoneurons arise from a low excitability state. J Neurosci 31, 5829–5840, doi:31/15/5829 [pii] 10.1523/JNEUROSCI.6363-10.2011 (2011). [PubMed: 21490224]
52. Mannelli LDC et al. Morphologic features and glial activation in rat oxaliplatin-dependent neuropathic pain. The Journal of Pain 14, 1585–1600 (2013). [PubMed: 24135431]
53. Kuo J, Lee R, Zhang L. & Heckman C. Essential role of the persistent sodium current in spike initiation during slowly rising inputs in mouse spinal neurones. The Journal of physiology 574, 819–834 (2006). [PubMed: 16728453]
54. Boyette-Davis JA, Walters ET & Dougherty PM Mechanisms involved in the development of chemotherapy-induced neuropathy. Pain management 5, 285–296 (2015). [PubMed: 26087973]
55. Sittl R. et al. Anticancer drug oxaliplatin induces acute cooling-aggravated neuropathy via sodium channel subtype Na(V)1.6-resurgent and persistent current. Proc Natl Acad Sci U S A 109, 6704–6709, doi:10.1073/pnas.1118058109 (2012). [PubMed: 22493249]
56. Descoeur J. et al. Oxaliplatin-induced cold hypersensitivity is due to remodelling of ion channel expression in nociceptors. EMBO molecular medicine 3, 266–278 (2011). [PubMed: 21438154]
57. Kagiava A, Tsingotjidou A, Emmanouilides C. & Theophilidis G. The effects of oxaliplatin, an anticancer drug, on potassium channels of the peripheral myelinated nerve fibres of the adult rat. Neurotoxicology 29, 1100–1106 (2008). [PubMed: 18845186]
58. Duflocq A, Chareyre F, Giovannini M, Couraud F. & Davenne M. Characterization of the axon initial segment (AIS) of motor neurons and identification of a para-AIS and a juxtapara-AIS, organized by protein 4.1 B. BMC biology 9, 66 (2011). [PubMed: 21958379]

59. Ling Y-Z et al. The inhibition of spinal synaptic plasticity mediated by activation of AMP-activated protein kinase signaling alleviates the acute pain induced by oxaliplatin. Experimental neurology 288, 85–93 (2017). [PubMed: 27856287]
60. Huang Z-Z et al. Cerebrospinal fluid oxaliplatin contributes to the acute pain induced by systemic administration of oxaliplatin. Anesthesiology: The Journal of the American Society of Anesthesiologists 124, 1109–1121 (2016).
61. Thompson SW, Davis LE, Kornfeld M, Hilgers RD & Standefer JC Cisplatin neuropathy. Clinical, electrophysiologic, morphologic, and toxicologic studies. Cancer 54, 1269–1275 (1984). [PubMed: 6088023]
62. Jacobs S. et al. Extracellular fluid concentrations of cisplatin, carboplatin, and oxaliplatin in brain, muscle, and blood measured using microdialysis in nonhuman primates. Cancer chemotherapy and pharmacology 65, 817–824 (2010). [PubMed: 19662415]
63. Jacobs SS et al. Plasma and cerebrospinal fluid pharmacokinetics of intravenous oxaliplatin, cisplatin, and carboplatin in nonhuman primates. Clinical cancer research 11, 1669–1674 (2005). [PubMed: 15746072]
64. Koppen C. et al. Quantitative imaging of platinum based on laser ablation-inductively coupled plasma-mass spectrometry to investigate toxic side effects of cisplatin. Metallomics 7, 1595–1603, doi:10.1039/c5mt00226e (2015). [PubMed: 26477751]
65. Guo P, Ma J, Li S. & Gallo JM Determination of paclitaxel in mouse plasma and brain tissue by liquid chromatography–mass spectrometry. Journal of Chromatography B 798, 79–86 (2003).
66. Strathmann FG et al. Residual platinum concentrations in post-cancer chemotherapy and healthy control populations using an automated, 96-well plate method and inductively coupled plasma mass spectrometry. The Journal of Applied Laboratory Medicine 1, 143–151 (2016). [PubMed: 33626787]
67. Carozzi V, Canta A. & Chiorazzi A. Chemotherapy-induced peripheral neuropathy: what do we know about mechanisms? Neuroscience letters 596, 90–107 (2015). [PubMed: 25459280]
68. Canta A, Pozzi E. & Carozzi VA Mitochondrial dysfunction in chemotherapy-induced peripheral neuropathy (CIPN). Toxics 3, 198–223 (2015). [PubMed: 29056658]
69. Areti A, Yerra VG, Naidu V. & Kumar A. Oxidative stress and nerve damage: role in chemotherapy induced peripheral neuropathy. Redox biology 2, 289–295 (2014). [PubMed: 24494204]
70. Han Y. & Smith MT Pathobiology of cancer chemotherapy-induced peripheral neuropathy (CIPN). Frontiers in pharmacology 4, 156 (2013). [PubMed: 24385965]
71. Fischer LR & Glass JD Axonal degeneration in motor neuron disease. Neurodegenerative Diseases 4, 431–442 (2007). [PubMed: 17934327]
72. Park SB et al. Acute abnormalities of sensory nerve function associated with oxaliplatin-induced neurotoxicity. Journal of clinical Oncology 27, 1243–1249 (2009). [PubMed: 19164207]
73. Krishnan AV, Lin CS-Y, Park SB & Kiernan MC Axonal ion channels from bench to bedside: a translational neuroscience perspective. Progress in neurobiology 89, 288–313 (2009). [PubMed: 19699774]
74. Rossi SL et al. Identification of early gene expression changes in primary cultured neurons treated with topoisomerase I poisons. Biochemical and biophysical research communications 479, 319–324 (2016). [PubMed: 27641670]
75. Leroy F, d'Incamps BL, Imhoff-Manuel RD & Zytnicki D. Early intrinsic hyperexcitability does not contribute to motoneuron degeneration in amyotrophic lateral sclerosis. Elife 3, e04046 (2014).
76. Martin E, Cazenave W, Cattaert D. & Branchereau P. Embryonic alteration of motoneuronal morphology induces hyperexcitability in the mouse model of amyotrophic lateral sclerosis. Neurobiology of disease 54, 116–126 (2013). [PubMed: 23466698]
77. Venugopal S, Hsiao C-F, Sonoda T, Wiedau-Pazos M. & Chandler SH Homeostatic dysregulation in membrane properties of masticatory motoneurons compared with oculomotor neurons in a mouse model for amyotrophic lateral sclerosis. Journal of Neuroscience 35, 707–720 (2015). [PubMed: 25589764]
78. Bélanger M, Allaman I. & Magistretti PJ Brain energy metabolism: focus on astrocyte-neuron metabolic cooperation. Cell metabolism 14, 724–738 (2011). [PubMed: 22152301]

79. Bellissimo MI et al. Superoxide dismutase, glutathione peroxidase activities and the hydroperoxide concentration are modified in the hippocampus of epileptic rats. Epilepsy research 46, 121–128 (2001). [PubMed: 11463513]

80. Calvo-Gallardo E. et al. Depressed excitability and ion currents linked to slow exocytotic fusion pore in chromaffin cells of the SOD1 G93A mouse model of amyotrophic lateral sclerosis. American Journal of Physiology-Cell Physiology 308, C1–C19 (2015). [PubMed: 25377090]

81. Ditting T. et al. Impaired excitability of renal afferent innervation after exposure to the inflammatory chemokine CXCL1. American Journal of Physiology-Renal Physiology 310, F364–F371 (2016). [PubMed: 26697980]

82. Dringen R. Metabolism and functions of glutathione in brain. Progress in neurobiology 62, 649–671 (2000). [PubMed: 10880854]

83. Hadzipasic M. et al. Selective degeneration of a physiological subtype of spinal motor neuron in mice with SOD1-linked ALS. Proceedings of the National Academy of Sciences 111, 16883–16888 (2014).

84. Kadoi J, Takeda M. & Matsumoto S. Prostaglandin E2 potentiates the excitability of small diameter trigeminal root ganglion neurons projecting onto the superficial layer of the cervical dorsal horn in rats. Experimental brain research 176, 227–236 (2007). [PubMed: 16850322]

85. Sareen D. et al. Targeting RNA foci in iPSC-derived motor neurons from ALS patients with a C9ORF72 repeat expansion. Science translational medicine 5, 208ra149–208ra149 (2013).

86. White FA, Jung H. & Miller RJ Chemokines and the pathophysiology of neuropathic pain. Proceedings of the National Academy of Sciences 104, 20151–20158 (2007).

87. Sisignano M, Baron R, Scholich K. & Geisslinger G. Mechanism-based treatment for chemotherapy-induced peripheral neuropathic pain. Nat Rev Neurol 10, 694–707, doi:10.1038/nrneurol.2014.211 (2014). [PubMed: 25366108]

88. Briones TL & Woods J. Chemotherapy-induced cognitive impairment is associated with decreases in cell proliferation and histone modifications. BMC neuroscience 12, 124 (2011). [PubMed: 22152030]

89. Wang X-M et al. Chemobrain: a critical review and causal hypothesis of link between cytokines and epigenetic reprogramming associated with chemotherapy. Cytokine 72, 86–96 (2015). [PubMed: 25573802]

Highlights

- Chemotherapy chronically impairs motoneuron repetitive firing.
- Deficits were restricted to intrinsic spike encoding properties contained in the central nervous system.
- Motoneurons exhibit reduced firing probability, unpredictable firing frequencies, and abolished control of firing-rate modulation
- Impaired balance in subthreshold NaPIC and Kv1 conductances exposed as likely biophysical mechanism.
- Impaired motoneuron firing necessarily produces chronic movement disorders and fatigue experienced by cancer survivors.

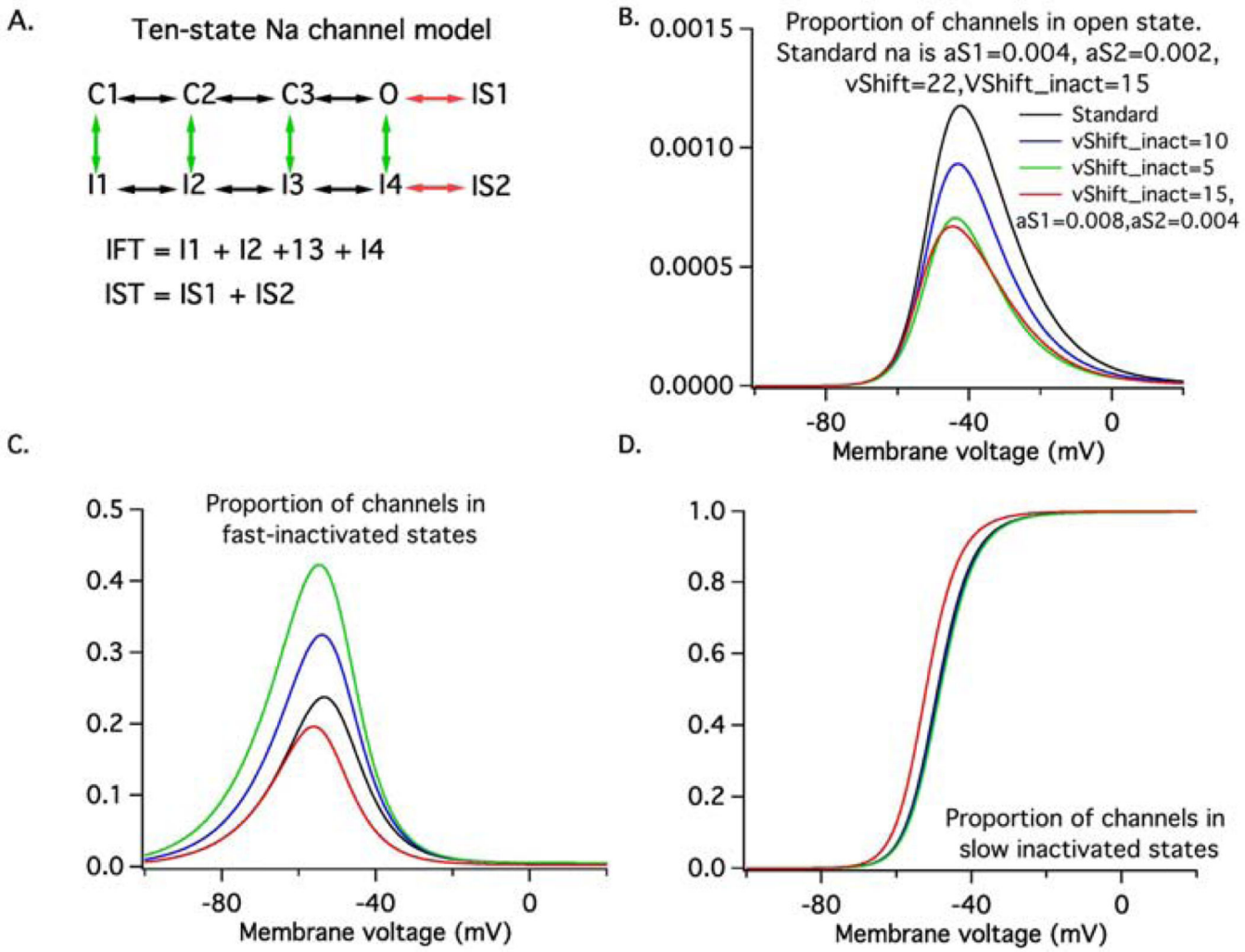

Figure 1. ***In Silico*** **Motoneuron Model.**

(A) Shows the ten-state model Na channel model. The green vertical arrows represent transitions to fast-inactivated states, whereas the red horizontal arrows represent transitions to slow-inactivated states. IFT represents the total occupancy of all fast-inactivated states whereas IST represents that of the slow-inactivated states. Shows the steady-state occupancy of the open (B), fast-activated (C) and slow-inactivated states (D) as a function of membrane voltage. The black lines represent the features of the standard model, the blue and green lines represent changes in fast-inactivation process produced by hyperpolarizing the fast-inactivation voltage-dependence by either 5 (blue) or 10 mV (green). The red lines represent changes in state occupancy produced by doubling the rate at which slow-inactivated states are entered. Note that the steady-state persistent Na current (open state occupancy) is nearly identical for the 10mV shift in fast-inactivation and for the faster entry into the slow-inactivated states. However, this state-state is reached at different rates in the two cases.

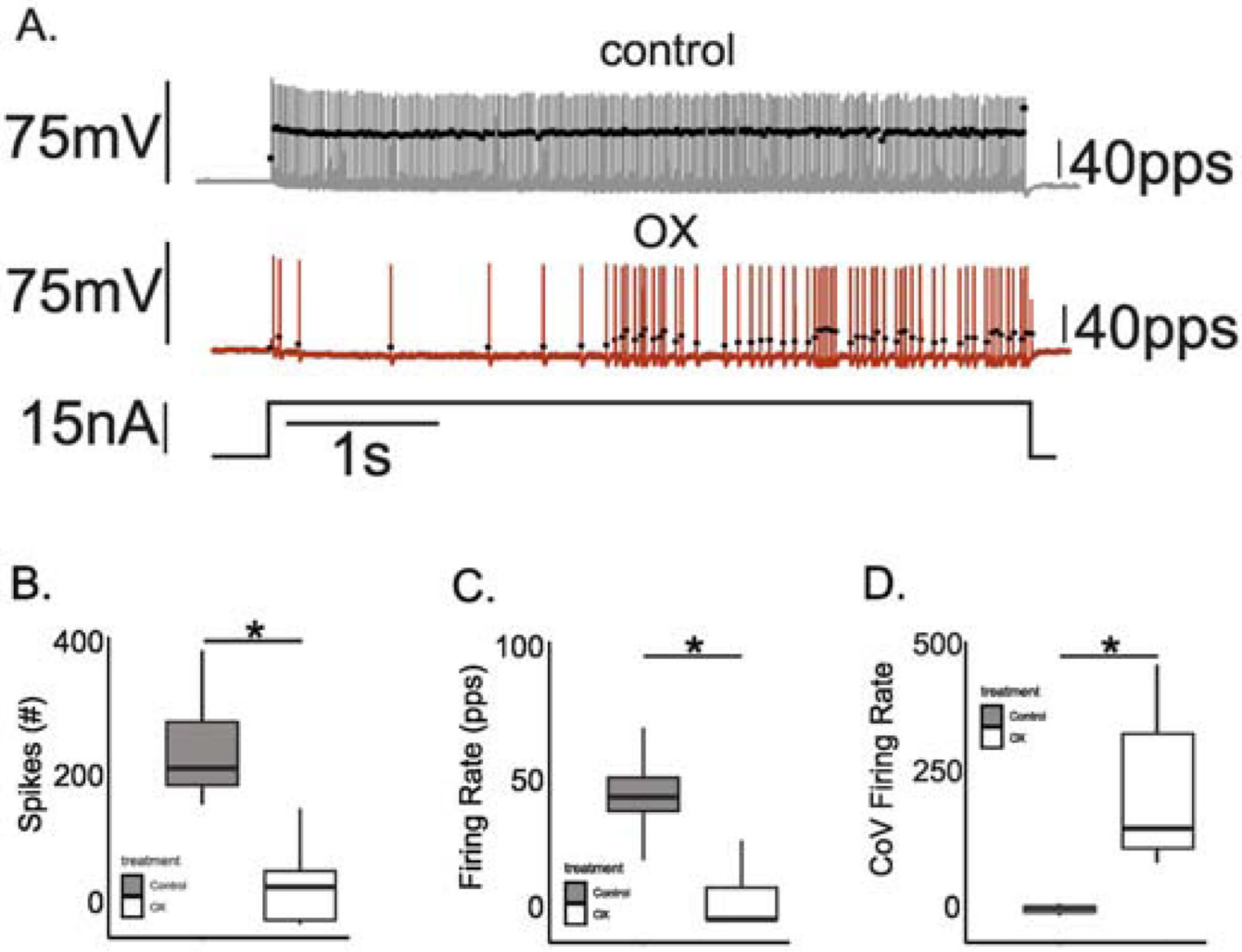

Figure 2. Chemotherapy Disrupted Repetitive Firing of Motoneurons.

(A) Records show representative instantaneous firing rates (filled black circles: pulses per second (pps)) superimposed on APs (grey lines: mV) recorded intracellularly from motoneurons acquired in a rat after 5 weeks after clinically relevant chemotherapy treatment (middle) and from a control rat (top) in response to matched depolarizing current injection (bottom trace: nA). Box and whisker plots compare (B) the total number of APs, (C) mean firing rate and (D) coefficient of variation in firing rate recorded for across all trials of 5 second depolarizing current injection in each treatment group. * indicates statistically significant differences between experimental groups as empirically derived from hierarchical Bayesian model (stan_glm): 95% highest density intervals do not overlap between groupwise contrasts.

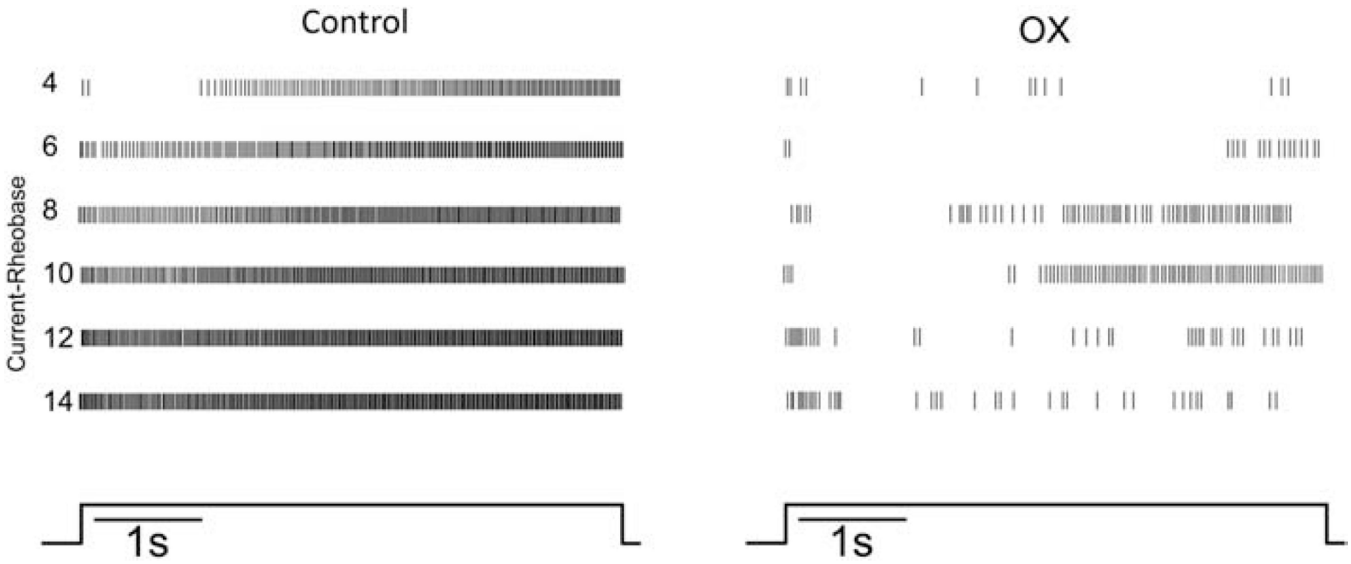

Figure 3. Firing disrupted at All Current Strengths.

Raster plots from representative control and OX motoneurons show firing responses to 5 sec trials of 5 sec current clamp (bottom trace). Vertical lines represent the timing of APs as they occur during each of the 5s trials aligned in rows of increasing depolarizing current from 4 to 14 nA above rheobase (current-rheobase). Selected motoneurons had comparable rheobases (control 10nA and OX 9nA).

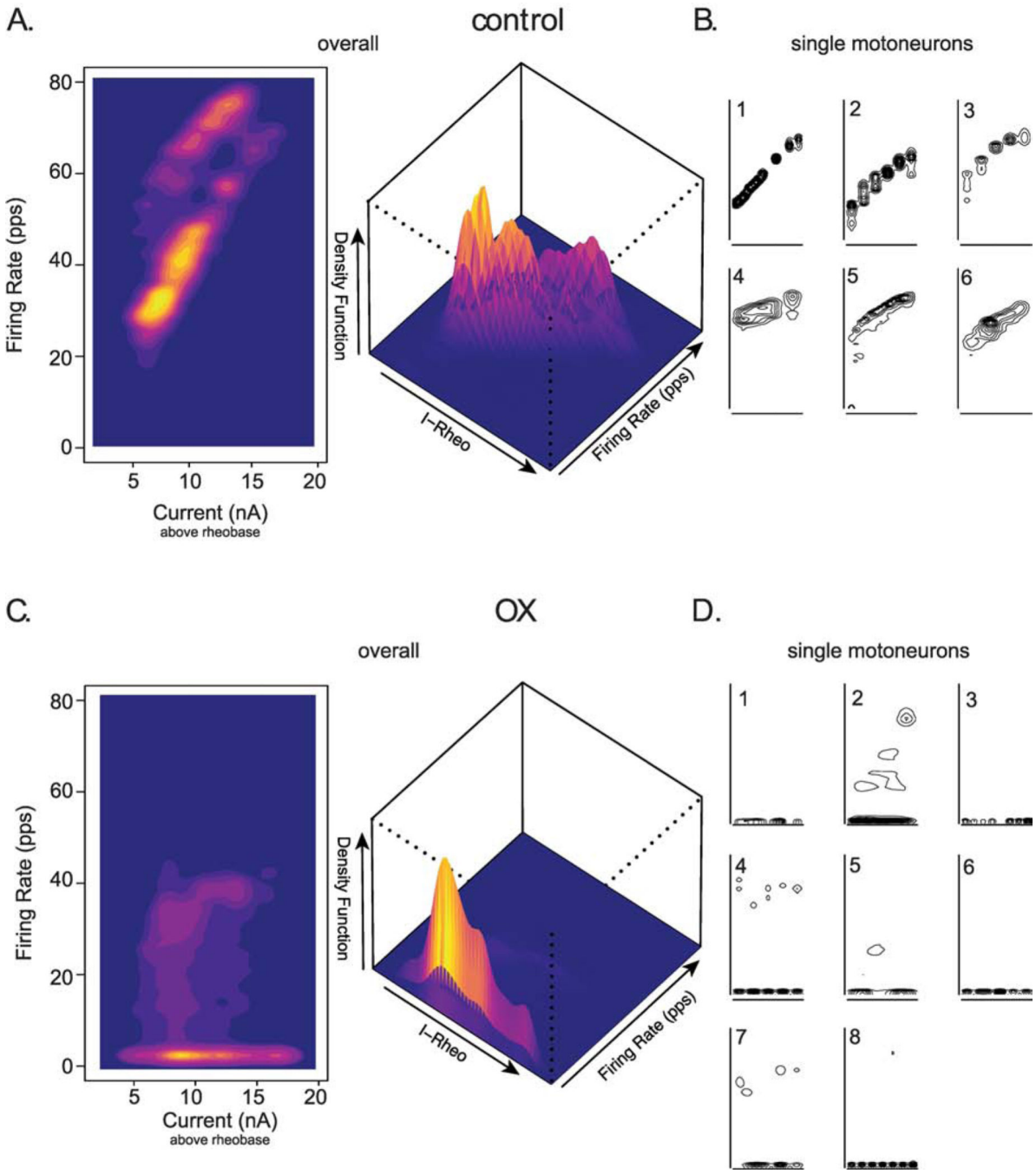

Figure 4. Firing Rate Modulation Nearly Eliminated.

(A and C) Two-dimensional plots (left) shows the population of control (A, n = 6) and chemotherapy (C, n = 8) motoneuron's capacity to modulate firing rate (frequency-current relationship: F-I) in response to varying levels of depolarizing current above rheobase (current-rheobase). Three-dimensional plot (right) highlights the density distribution of raw data across all injected currents levels. Narrowing topographical lines in B and D and hotter colors in A and C indicate higher density and correspond to higher peak values in plot to

right. B and D show F-I plots from individual motoneurons comprising control and chemotherapy plots in A and C respectively.

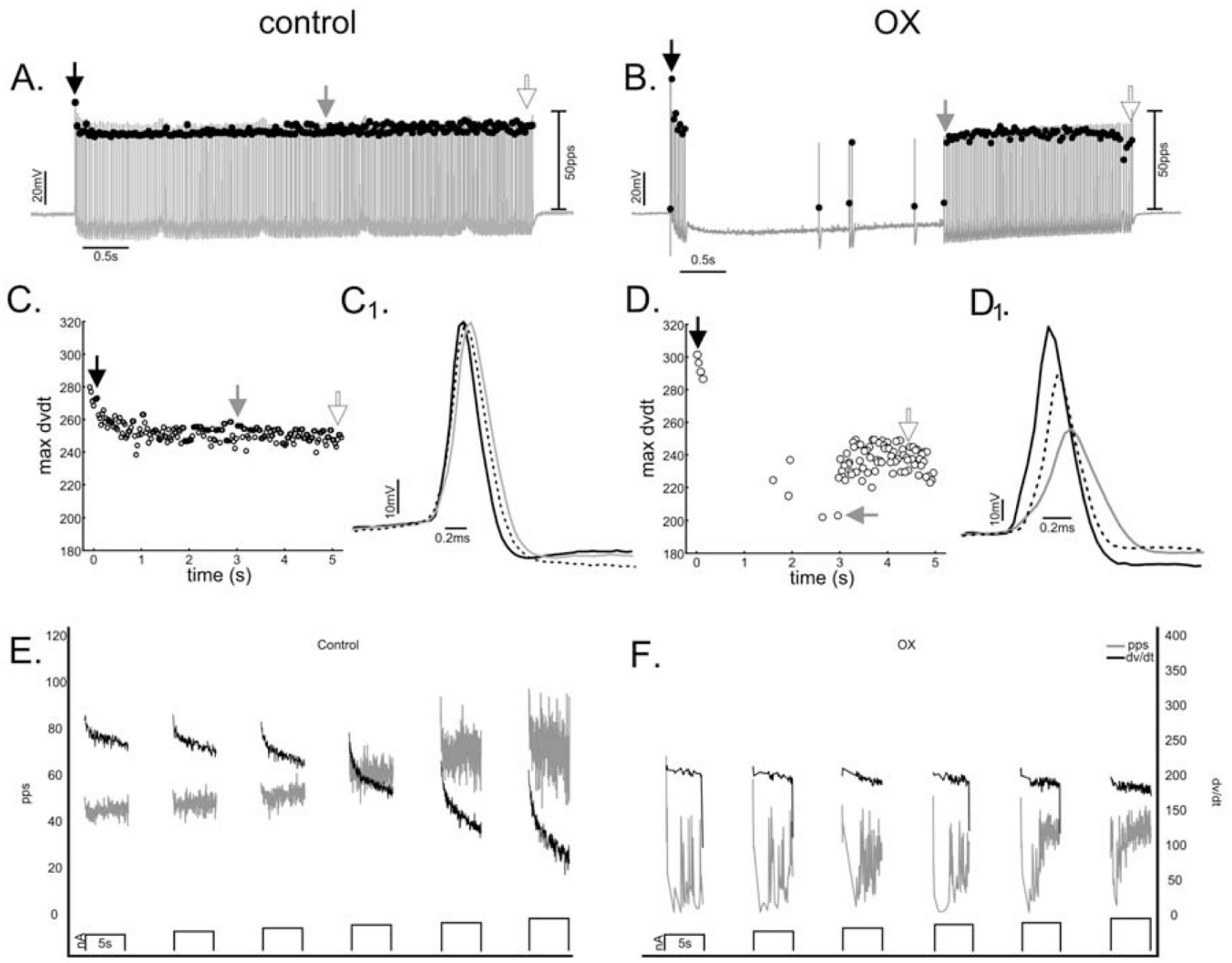

Figure 5. AP dV/dt not Predictive of Firing Cessation and Resumption.

(A and B) Instantaneous firing rate (filled black circles: pulses per second (pps)) superimposed on APs (grey lines: mV) recorded from (A) control and (E) OX motoneurons during current clamp. (C and D) Scatter plots of dv/dt extracted from all APs illustrated in records A and B, respectively. Insets show time-expanded APs superimposed and identified by black, dotted and grey lines corresponding to their positions during repetitive firing indicated, respectively, as black, open, and grey arrows in (A,B and C,D). (E and F) Traces of firing rate (grey lines relative to left y axis) and dV/dt (black lines relative to right y axis) for 6 trials each of increasing current (3–8 nA above rheobase current bottom traces on x axis) for (E) one control and (F) one OX motoneuron.

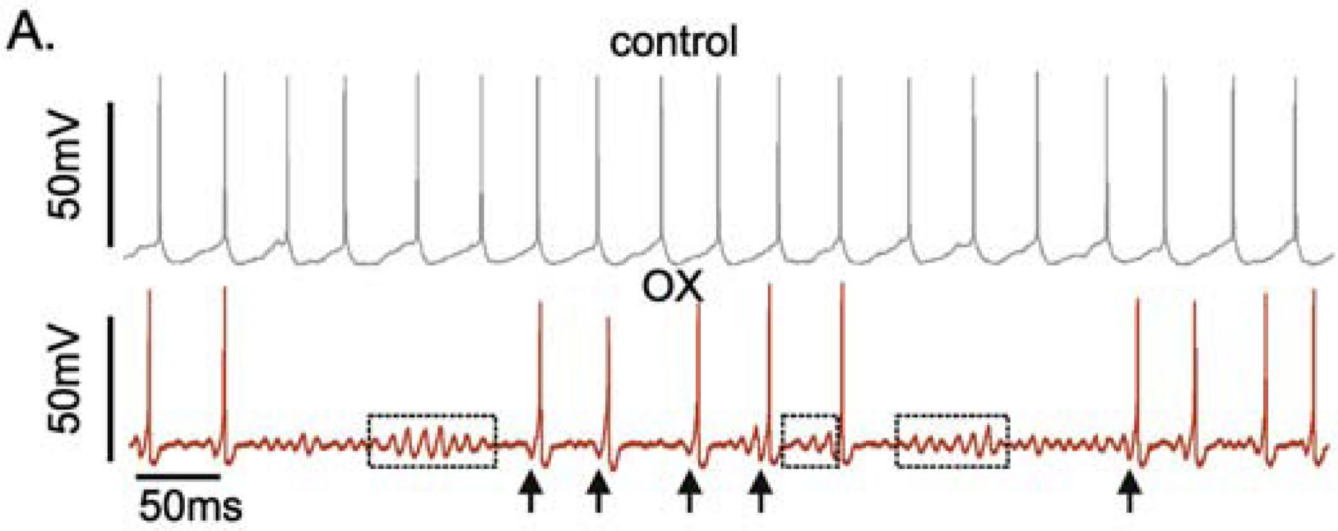

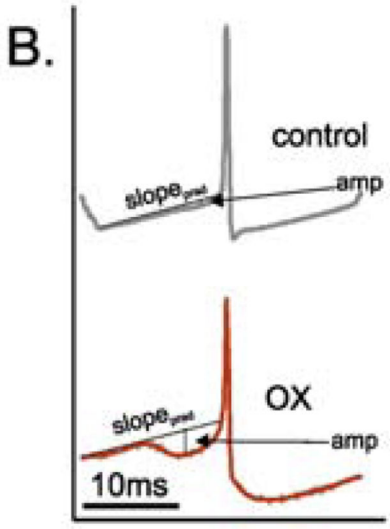

C.

	control	OX
$slope_{avg}$ (mv/s)	6.06±.79	1.45±.29*
$slope_{pred}$ (mv/s)	7.53±.9	4.85±.48*
amp (mv)	1.5±0.2	3.2±0.6*

Figure 6. Subthreshold Membrane Potential Oscillations.

(A). Shows representative intracellular records of membrane potential for control (top: grey) and OX (bottom: red) motoneurons in response to matched depolarizing current injection. In record from OX motoneuron, dotted boxes outline prominent subthreshold oscillations and arrows point to hyperpolarization immediately preceding AP, designated pre-spike hyperpolarization. (B) Spike-triggered averages of membrane potential preceding all APs in current-matched trials control and OX motoneurons illustrating pre-spike hyperpolarization. (C) shows the observed (top) and predicted (middle) voltage slopes for the 15ms preceding AP threshold along with the average amplitude in pre-AP hyperpolarization (bottom).

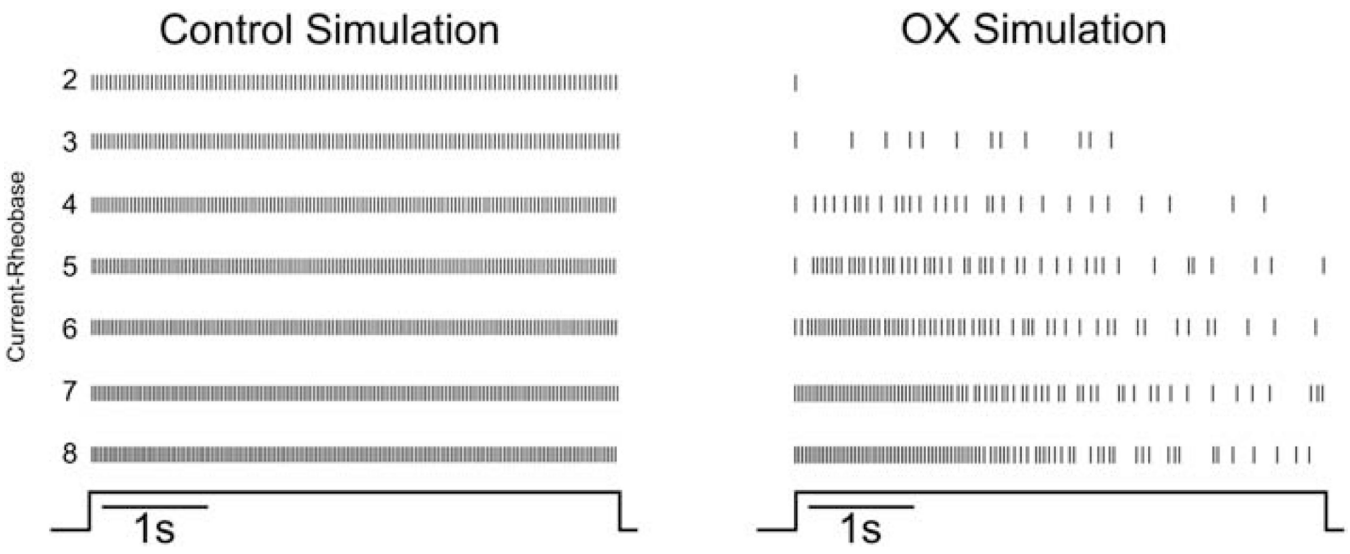

Figure 7. Modulation of Subthreshold Kinetics Reproduces Erratic Firing.

Raster plots from simulated control and simulated OX motoneurons show firing responses to depolarizing current that are analogous to experimentally observed data in Fig. 4. Vertical lines represent the timing of action potentials as they occur during each of the 5s trials. Each horizontal trace represents a single 5s trial as the depolarizing current is increased from 2 to 8nA above rheobase (current-rheobase). Control motoneuron firing behavior was modeled with both a high level of NaPIC and a low level of Kv1 (0.002 S/cm2, bottom panel). OX motoneuron firing was modelled by altering the level of Kv1 (0.006 S/cm2) and lowering NaPIC. In this case, the decrease in NaPIC resulted from increased slow Na inactivation and exhibited a stuttering firing pattern over a large range, from just a few nA above rheobase (I-rheobase = 9 nA) up to 21 nA above rheobase (the highest current level tested).

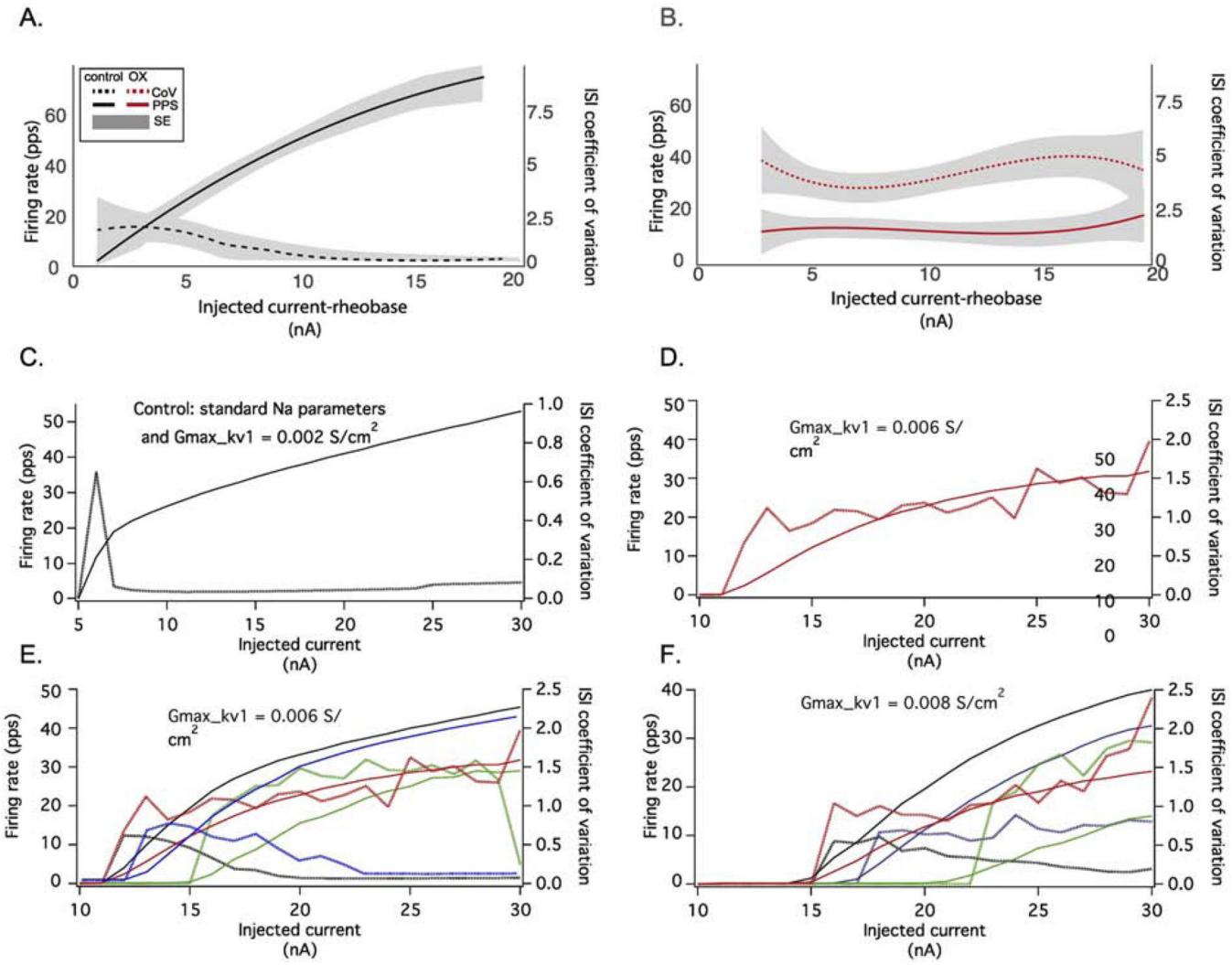

Figure 8. Erratic Firing in Conductance Parameter Space.

A and B show the average firing rates produced by a 5 sec injected current step (solid lines) along with the coefficient of variation (CoV) of the interspike intervals (ISI: dotted lines) for different levels of injected current for experimentally observed control (A) and OX data (B). (C) Control motoneuron firing behavior was modeled with both a high level of Na current and a low level of Kv1 (0.002 S/cm2). (D) OX motoneuron firing was modelled by increasing the level of Kv1 (0.006 S/cm2) and the amount of slow inactivation. In this case, the model had increased slow inactivation and exhibited a stuttering firing pattern of a large range, from just a few nA above rheobase (I-rheobase = 9 nA) up to 21 nA above rheobase (the highest current level tested) and qualitatively matched experimentally observed trends, although rate modulation was blunted but largely preserved. E and F show the relationship between CoV and firing rate over two fixed levels of Kv1 0.006 S/cm2 (E) and 0.008 S/cm2, and for different levels of NaPIC: the standard level (black), decreased due to a 5 mV or 10 mV shift in fast inactivation (blue and green), and increased due to an increase in slow Na inactivation. In all model configurations, the firing rate increased monotonically with the level of injected current, in contrast to the experimental data (B).

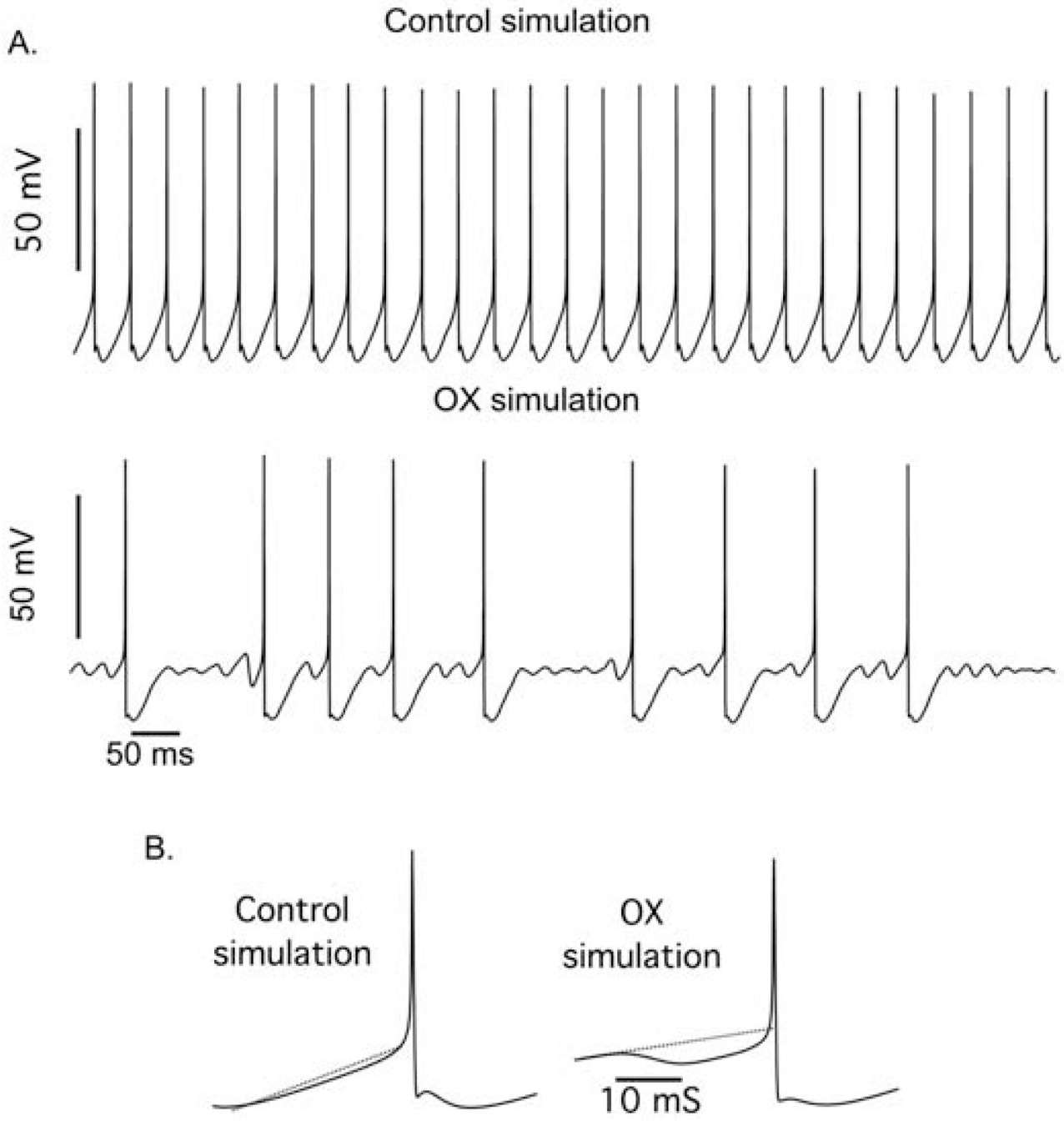

Figure 9. Modeling Subthreshold Oscillations and Pre-Spike Hyperpolarization.

(A). Intracellular voltage records from a simulated control and OX motoneuron. (B) Spike-triggered average (STA) from entire 5s current injection trial shows the average membrane voltage (mV) immediately preceding spiking for the control and OX simulation.

Table 1.

Action potential and passive properties of motoneurons in control and chemotherapy rats.

	Control	OX
Resting potential (mV)	73.16 ± 1.18	73.64 ± 2.51
Conductance (μS)	0.53 ± 0.15	0.65 ± 0.25
AHP ½ decay (ms)	12.87 ± 1.08	10.62 ± 0.74
AHP amplitude (mV)	2.09 ± 0.35	1.72 ± 0.346
AP amplitude (mV)	79.43 ± 2.97	73.29 ± 2.19
AP width (ms)	0.415 ± 0.016	0.378 ± 0.011
dV/dt max (mV/ms)	266.58 ± 25.6	262.87 ± 12.5
dV/dt min (mV/ms)	−204.65 ± 14.7	−208.87 ± 13.7
Rheobase (nA)	10.57 ± 2.26	14.5 ± 2.66

Values are means ± SE. Control, n = 7 motoneurons from 6 rats. Chemotherapy, n = 8 motoneurons from 5 rats. AHP: afterhyperpolarization, AP: action potential. No statistically significant differences between experimental groups as empirically derived from hierarchical Bayesian model (stan_glm).